PALEOCEANOGRAPHY, VOL. 13, NO. 5, PAGES 502-516, OCTOBER 1998

Optimal sites for coral-based reconstruction of global sea surface temperature

Michael N. Evans,[1] Alexey Kaplan and Mark A. Cane[1]

Lamont-Doherty Earth Observatory of Columbia University, Palisades, New York

Abstract. We determine the structure of a network of sites from which coral-based, proxy measurements of sea surface temperature (SST) variability minimize the error in a reconstruction of the large-scale features of the global SST field. For a wide range of coral-derived SST observational error and several minimization criteria, sites in the equatorial oceans, especially the central and eastern equatorial Pacific, best minimize the error in the reconstruction. If the observational error is sufficiently low, additional optimal sites are in selected subtropical locations. If the observational error is high, the error is minimized by resampling the most important equatorial sites. The marginal return on additional sites diminishes rapidly and is not sensitive to the size of the observational error: two sites reduce the analysis error by half as much as 10 sites, while the first 6-7 sites achieve half the error reduction of all 65 sites in the analysis domain. In the extratropics the reduction of reconstruction error is small and gradual, while error in the tropical Pacific is sharply reduced by 2-3 sites and gradually thereafter. These results suggest that a limited set of redundantly sampled sites with uncorrelated and low observational error ($\approx$0.3°-0.6°C) will provide the best approach to reconstruction of large-scale features of the SST field from coral data for the preinstrumental period.

1. Introduction

As the available instrumental record is limited in most places to the past 150 years or less [*Bottomley et al.*, 1990], sea surface temperature (SST) field reconstruction from proxy measurements is the only technique by which historical variability may be placed in the context of natural variability. However, construction of spatially and temporally extensive proxy records is challenging. Not only do we currently lack the means by which to sample large portions of the ocean, but the expense and difficulty of constructing and testing proxy climate records precludes comprehensive sampling. Suppose, instead, that we seek to reconstruct a multicentury record of the large-scale features of a climate field such as SST, using only a sparse observational network of proxy observations. Such proxy estimates of SST can be made at high temporal resolution from the stable isotopic or trace metal composition of the aragonite formed by massive reef corals [*Dunbar et al.*, 1994; *Quinn et al.*, 1998; *Charles et al.*, 1997; *Evans et al.*, 1998]. Given a possible set of locations at which we can construct such proxy time series, what combination of sites best captures global SST variability?

The general problem is the optimization of an oceanographic experimental array design [*Bretherton et al.*, 1976; *Bretherton and McWilliams*, 1980; *McPhaden et al.*, 1984; *Barth and Wunsch*, 1990; *Miller*, 1990; *Bennett*, 1990; *Hayes et al.*, 1991; *Bennett*, 1992; *Hackert et al.*, 1997], and the approach outlined here might be used to identify optimal sampling schemes for a wide range of variables and systems. The specific question involving paleoclimatic reconstruction is similar to that posed by *Bradley* [1996]. He considered a more general set of proxy records of climate and based his determination of optimal sites on existing data and their correlation with global mean annual air temperatures from historical data and coupled atmosphere-ocean model results. Figure 1 illustrates the approach intuitively; with respect to the coral-based reconstruction of global mean annual sea surface temperature, sites within contours of highest correlation will individually provide the best reconstruction of SST. However, it is not necessarily the case that the best network is composed of the sites having the highest individual correlations with global temperature. Having resolved the information highly correlated with the best site, the reconstruction of global mean temperature may be most improved by adding a site that resolves additional features of SST variability, although it is less correlated with global SST than other sites. For example, if the best single site is located in the tropical Pacific, nearby sites may not provide as much nonredundant information as a site in the tropical Indian Ocean sector. Hence here we adopt an approach based on principles of inverse modeling which objec-

[1]Also at Department of Earth and Environmental Sciences, Columbia University, New York, New York.

Paper number 98PA02132.
0883-8305/98/98PA-02132$12.00

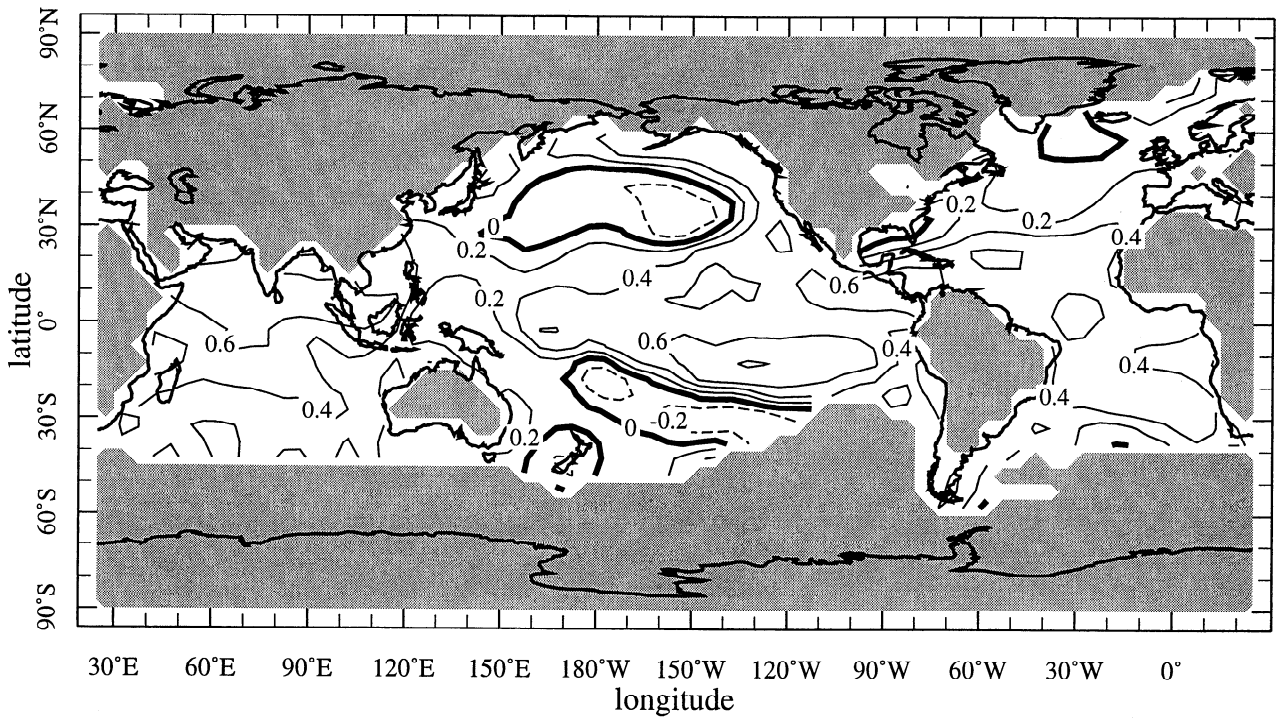

Figure 1. Correlation r of annual mean sea surface temperature (SST) anomaly with the global mean sea surface temperature for the period 1856-1991. The contour interval is 0.2 correlation units. Data are from *Cane et al.* [1997] and *Kaplan et al.* [1998]. The shaded regions show areas not included in the analysis grid; our global grid excludes much of the Arctic and Southern Oceans.

tively minimizes the estimated error in a reconstruction of the large-scale modes of spatial SST variability. In addition to estimation of the global mean temperature we will consider the entire class of optimal networks that may, for example, be used to best estimate area means (e.g., SST indices) of interest.

This paper presents the best set of sites from which to reconstruct the global SST temperature field from a sparse, as yet unrealized, network of coral-based time series. The analysis is based on the error formulation for optimal interpolation of sea surface temperature data via a reduced space of spatial SST covariance patterns. This approach to climate field reconstruction, which was first proposed by *Cane et al.* [1996] and *Kaplan et al.* [1997, 1998] for reconstruction of sea level height and sea surface temperature fields from spatially and temporally heterogeneous observations, is here applied to the problem of SST field reconstruction from a sparse network of coral-derived proxy data. In section 2 we describe the optimal interpolation field reconstruction technique. We next explain its application to the problem posed (section 3), and emphasize the assumptions made in the analysis (section 4). In section 5 we present networks of sites which minimize the field reconstruction error for specified input parameters, including some examples of networks derived from other minimization criteria, and discuss the implications of these results.

2. Optimal Interpolation Field Reconstruction Technique

Optimal interpolation (OI) is an inverse technique for finding the best fit field, in a least squares sense, to both a sparse observational network of data and a description, or model, of how the field varies. Errors are admitted in both the observations and the model. A cost function, consisting of the appropriately weighted squared errors in the observations and the model, is then formulated. Minimization of the cost function produces the field which best fits the data and the model given prior estimates of how precisely the model and observations are known. The error in the OI-analyzed field produced in this manner is a function of the observational error, the model error, and the extent to which the field is resolved by the observations.

Consider the example [*Ghil et al.*, 1981; *Ghil and Malanotte-Rizzoli*, 1991; *Cane et al.*, 1996] in which we seek an estimate for the sea surface temperature anomaly T, at one point in time and space. Suppose we have an observation, T_o, with expected mean error = zero and expected error variance σ_o^2, which is related to T by the measurement operator h: $T_o = h(T)$. The measurement operator is the relationship between what is actually measured (T_o) and the desired property estimate T. For instance, h may select the observation

point and interpolate to it from the grid on which we wish to estimate T, and it may also translate to the measurement (e.g., $\delta^{18}O$) from the property of interest (e.g., temperature). Suppose, in addition to our observation T_o, we also have a model estimate $T_m = a(T)$, also with zero expected error and with expected error variance σ_m^2. Let us assume that h and a are linear and that the model directly estimates T: $T_o = hT$, $T_m = aT$, and $a = 1$. Further, we assume that T_o and T_m are unbiased; that is, the average of repeated observations or model estimates will approach the true value, T. Finally, we assume that the error variances are known to be σ_o^2 for the observation and σ_m^2 for the model. Then we can write a least squares cost function consisting of the observational and model residuals with respect to T:

$$S = [(hT - T_o)/\sigma_o]^2 + [(T - T_m)/\sigma_m]^2$$

Minimization of S with respect to T gives the optimal estimate of T, $\hat{T}$:

$$\hat{T} = (h^2\sigma_o^{-2} + \sigma_m^{-2})^{-1}(hT_o\sigma_o^{-2} + T_m\sigma_m^{-2})$$

In this case, $\hat{T}$ is an average of the observation and model estimates of T, weighted by the errors in T_m and T_o. For example, if the observation is known to greater accuracy than the model result, the solution $\hat{T}$ will approach the value of T_o. The analysis error is

$$P = (h^2\sigma_o^{-2} + \sigma_m^{-2})^{-1}$$

Now suppose instead of this simple case that we have many observations in space and a model estimate of T everywhere. $\mathbf{T}$, $\mathbf{T_o}$, and $\mathbf{T_m}$ are then fields and can be written as vectors. In matrix notation, let $\mathbf{H}$ be the map from $\mathbf{T}$ to $\mathbf{T_o}$ and let $\mathbf{R_o}$ and $\mathbf{R_m}$ be the observational and model error covariance matrices, respectively. Superscript T will denote the matrix transpose. Then the optimal estimate $\hat{\mathbf{T}}$ is

$$\hat{\mathbf{T}} = \mathbf{P}(\mathbf{H}^{\mathbf{T}}\mathbf{R_o}^{-1}\mathbf{T_o} + \mathbf{R_m}^{-1}\mathbf{T_m}) \quad (1)$$

where $\mathbf{P}$, the error covariance of the optimal estimate, is

$$\mathbf{P} = (\mathbf{H}^{\mathbf{T}}\mathbf{R_o}^{-1}\mathbf{H} + \mathbf{R_m}^{-1})^{-1} \quad (2)$$

Kaplan et al. [1998] recently applied least squares optimal interpolation and smoothing techniques to the analysis of a near-global, historical sea surface temperature anomaly data set. For their model they used the relatively well-observed 1950-1991 period to construct the spatial SST anomaly covariance matrix. Since only the large-scale modes of variability are known, and to reduce computational expense of the procedure, they retained the leading 80 empirical orthogonal functions (EOFs) of the covariance matrix. These 80 modes together describe ≈75% of the SST anomaly covariance in the original data; the remaining 25% has small spatial scale and is poorly resolved above the level of intrabox variability [*Kaplan et al.*, 1998]. The resulting analyzed fields are a best fit to both the available observations and this statistical model of spatial covariance of large-scale sea surface temperature anomaly.

In this case the "model" is that the SST takes its climatological value; that is, the anomaly is zero. The least squares cost function S that may be used to minimize the misfit between the analyzed and observed SST anomaly fields and between the analyzed field and the model is

$$S(\mathbf{T}) = (\mathbf{T} - \mathbf{T_o})^{\mathbf{T}}\mathbf{R}^{-1}(\mathbf{T} - \mathbf{T_o}) + \mathbf{T}^{\mathbf{T}}\mathbf{C}^{-1}\mathbf{T} \quad (3)$$

Here $\mathbf{R}$ is the error covariance of the observations and $\mathbf{C}$ is the spatial SST anomaly covariance. Note that $\mathbf{C}$ is the error covariance in the model estimate of zero anomaly.

We can also write $\mathbf{T}$ as the linear combination of a small number of EOFs [*Kaplan et al.*, 1997, 1998], which retain most of the SST anomaly variance.

$$\mathbf{T} = \mathbf{HE}\boldsymbol{\alpha} + \mathbf{error} \quad (4)$$

Here $\mathbf{H}$ is the measurement operator, $\mathbf{E}$ is the matrix whose columns are the retained EOF patterns, $\boldsymbol{\alpha}$ is the vector containing the temporal amplitudes of $\mathbf{E}$, and the error is due to the reduction in the dimension of the EOF space. $\mathbf{H}$ is a vector representing the locations of SST observations, with point value 1 in the ith row representing a grid point from which SST is observed and zero otherwise. The cost function (equation 3) can be re-written in terms of $\mathbf{E}$ and $\boldsymbol{\alpha}$:

$$S(\boldsymbol{\alpha}) = (\mathbf{HE}\boldsymbol{\alpha} - \mathbf{T_o})^{\mathbf{T}}\mathbf{R}^{-1}(\mathbf{HE}\boldsymbol{\alpha} - \mathbf{T_o}) + \boldsymbol{\alpha}^{\mathbf{T}}\boldsymbol{\Lambda}^{-1}\boldsymbol{\alpha} \quad (5)$$

where $\boldsymbol{\alpha}$ is the vector containing the temporal amplitudes of $\mathbf{E}$, $\mathbf{T_o}$ is the matrix of observations, $\boldsymbol{\Lambda}$ is the diagonal matrix whose elements contain the retained eigenvalues of $\mathbf{E}$, and $\mathbf{R}$ is the error covariance matrix. $\mathbf{HE}$ is the map from the principal components of the retained EOFs to the field $\mathbf{T}$. The first term in S is the squared difference between the OI solution and the observed SST anomaly, while the second term represents the energy in the modes of the OI solution, weighted by the inverse of the eigenvalues of the SST anomaly covariance (i.e., the covariance matrix in EOF space). Since the reduced space approach throws away ≈25% of the variance in the SST anomaly covariance matrix, $\mathbf{R}$ includes both observational error and EOF space reduction error terms:

$$\mathbf{R} = \mathbf{R_o} + \mathbf{HE'\Lambda'E'}^{\mathbf{T}}\mathbf{H}^{\mathbf{T}} \quad (6)$$

where $\mathbf{R_o}$ is the diagonal matrix whose elements contain the observational error variance of the data, ϵ^2, $\mathbf{E'}$ is the matrix containing the discarded EOFs, and $\boldsymbol{\Lambda'}$ contains their respective eigenvalues. The second term

in (6) represents the error incurred by reducing the EOF space.

Minimization of S defined by (5) gives the optimal reduced space estimate of the temperature field $\hat{\mathbf{T}} = \mathbf{E}\hat{\boldsymbol{\alpha}}$:

$$\hat{\mathbf{T}} = \mathbf{E}\hat{\boldsymbol{\alpha}} = \mathbf{E}\mathbf{P}\mathbf{E}^{\mathrm{T}}\mathbf{H}^{\mathrm{T}}\mathbf{R}^{-1}\mathbf{T}_{\mathrm{o}} \tag{7}$$

The error covariance in $\hat{\boldsymbol{\alpha}}$ is given by

$$\mathbf{P} = (\mathbf{E}^{\mathrm{T}}\mathbf{H}^{\mathrm{T}}\mathbf{R}^{-1}\mathbf{H}\mathbf{E} + \boldsymbol{\Lambda}^{-1})^{-1} \tag{8}$$

while the error in $\hat{\mathbf{T}}$ is $\mathbf{E}\mathbf{P}\mathbf{E}^{\mathrm{T}}$.

3. Site Optimization for SST Reconstruction From Corals

The previous section showed that the OI error covariance (equation (2)) may be recast as a function of the spatial SST anomaly covariance, the EOF variances, the measurement operator $\mathbf{H}$, and the observational and space-reduction error (equation (8)). Now we consider the case in which the observational data consist of a spatially sparse network of hypothetical coral time series. The measurement operator $\mathbf{H}$ is taken to be a sparse matrix of locations of coral observational sites on the SST anomaly grid, with point value 1 in the ith row representing a location where the ith coral site is found and zero otherwise. We can now find the set of sites $\hat{\mathbf{H}}$ which minimizes $\mathbf{P}$, given $\mathbf{E}$, $\boldsymbol{\Lambda}$, and $\mathbf{R}$. That the sampling from the SST field is derived from proxy measurements on corals imposes certain constraints on the problem, which are outlined below.

3.1. Locations of Potential Sites

Growth of corals suitable for our purpose is limited to regions with appropriate ranges of light, nutrients, sea surface temperature, and salinity [*Sorokin*, 1993]. Coral colonies also require a substrate on which to establish themselves. These constraints limit the number of possible sites from which coral information may be obtained [*Darwin*, 1962]. For this analysis we selected 65 possible $5^{\circ}\times5^{\circ}$ grid boxes from a total of 1207 in the grids of the Global Ocean Surface Temperature Atlas (GOSTA) [*Bottomley et al.*, 1990] and Kaplan analyses on the basis of observations of coral colonies from *Bryan* [1952] and the International Center for Living Aquatic Resources Management database (ReefBase: A global database on coral reefs and their resources, http://www.cgiar.org/iclarm/resprg/reefbase, 1997, hereafter referred to as *ICLARM* [1997]) (Figure 2, solid boxes; Table 1). Coral-based time series collected from anywhere within these $5^{\circ}\times5^{\circ}$ grid boxes will be assumed to contain the same information as time series from the center of the grid point. This approx-

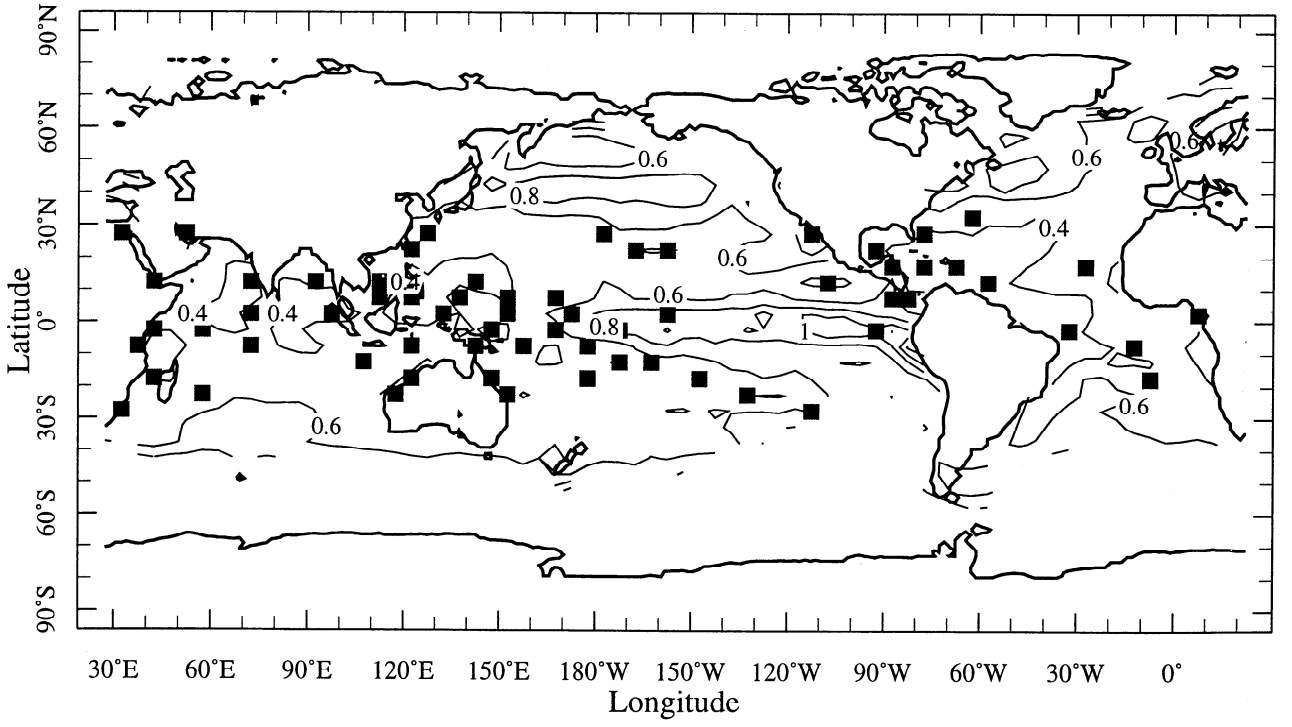

Figure 2. Location of the 65 $5^{\circ}\times5^{\circ}$ grid boxes in which coral samples suitable for climate reconstructions are assumed to be recoverable (solid squares); coral colonies suitable for extraction of paleoclimatic information are generally found within 30 m of the sea surface and within 30° latitude of the equator. Contours give SST anomaly signal amplitude (°C RMS) in the reduced empirical orthogonal function (EOF) space used in this analysis [*Kaplan et al.*, 1998].

Table 1. Database of Potential Sites for Reconstruction of Sea Surface Temperature (SST) From Corals

Location Name	Abbreviated Name	Longitude	Latitude	Grid Longitude	Grid Latitude
Abraham Reef	ABR	152.5°E	22.1°S	152.5°E	22.5°S
Adele	ADE	123.2°E	15.5°S	117.5°E	17.5°S
Admiralty Island	ADM	147.3°E	2.6°S	147.5°E	2.5°S
Andaman Island	AND	92.5°E	10.2°N	92.5°E	12.5°N
Ascension Island	ASC	14.6°W	7.2°S	12.5°W	7.5°S
Aqaba	AQA	35.0°E	29.5°N	32.5°E	27.5°N
Bahamas	BAH	77.0°W	26.5°N	77.5°W	27.5°N
Barbados	BAR	59.6°W	13.2°N	57.5°W	12.5°N
Belize	BEL	88.0°W	17.7°N	87.5°W	17.5°N
Bermuda	BER	64.7°W	32.3°N	62.5°W	32.5°N
Barrow Reef	BRW	115.3°E	20.7°S	117.5°E	22.5°S
Chiriqui	CHI	82.3°W	8.0°N	82.5°W	7.5°N
Christmas Island	CHR	105.6°E	10.6°S	107.5°E	12.5°S
Clipperton	CLI	109.2°W	10.3°N	107.5°W	12.5°N
Cape Verde Island	CVI	26.0°W	16.0°N	27.5°W	17.5°N
Isl. del Coco	COC	87.3°W	5.6°N	87.5°W	7.5°N
Diego Garcia	DGA	72.5°E	7.3°S	72.5°E	7.5°S
Easter Island	EAS	109.3°W	27.2°S	112.5°W	27.5°S
Felidhu	FEL	73.5°E	3.5°N	72.5°E	2.5°N
Fiji	FIJ	178.4°E	18.2°S	177.5°E	17.5°S
Funafuti	FUN	179.2°E	8.5°S	177.5°E	7.5°S
Galapagos	GAL	90.4°W	0.7°S	92.5°W	2.5°S
Gambier	GAM	134.6°W	23.1°S	132.5°W	22.5°S
Gardner	GAR	168.2°W	24.9°N	167.5°W	22.5°N
Guam	GUA	144.7°E	13.3°N	142.5°E	12.5°N
Guaymas	GYM	111.0°W	27.8°N	112.5°W	27.5°N
Hawaii	HAW	157.9°W	21.0°N	157.5°W	22.5°N
Ishigaki	ISH	124.3°E	24.5°N	122.5°E	22.5°N
Jamaica	JAM	77.3°W	18.3°N	77.5°W	17.5°N
Juan de Nova	JDN	42.8°E	17.0°S	42.5°E	17.5°S
Kanton	KAN	171.7°W	2.8°S	172.5°W	2.5°S
Kapingamarangi	KAP	154.7°E	0.6°N	152.5°E	2.5°N
Kish	KIS	54.0°E	26.5°N	52.5°E	27.5°N
Kiritimati	KIR	157.3°W	2.0°N	157.5°W	2.5°N
Kwajalein	KWA	167.3°E	9.5°N	167.5°E	7.5°N
Lakshadeep	LAK	73.7°E	11.2°N	72.5°E	12.5°N
Manihiki	MAN	161.0°W	10.4°S	162.5°W	12.5°S
Maza	MAZ	143.2°E	9.2°S	142.5°E	7.5°S
Midway	MID	177.3°W	28.3°N	177.5°W	27.5°N
Nauru	NAU	167.0°E	0.5°S	167.5°E	2.5°S
Nine Mile Reef	NMR	32.7°E	27.4°S	32.5°E	27.5°S
Okinawa	OKI	128.0°E	26.5°N	127.5°E	27.5°N
Palau	PAL	131.7°E	2.7°N	132.5°E	2.5°N
Penju	PEN	96.2°E	3.7°N	97.5°E	2.5°N
Philippines	PHI	123.5°E	13.6°N	122.5°E	12.5°N
Puerto Rico	PUE	66.2°W	17.9°N	67.5°W	17.5°N
Reunion	REU	55.5°E	21.1°S	57.5°E	22.5°S
Rocas Reef	ROC	33.8°W	3.9°S	32.5°W	2.5°S
Samoa	SAM	170.7°W	14.3°S	172.5°E	12.5°S
Seychelles	SEY	55.5°W	4.6°S	57.5°E	2.5°S
Solomon Is.	SOL	157.0°E	7.9°S	157.5°E	7.5°S
Somalia	SOM	41.9°E	1.2°S	42.5°E	2.5°S
Spratly Isl	SPR	113.0°E	7.9°N	112.5°E	7.5°N
St. Helena	STH	5.7°W	16.0°S	7.5°W	17.5°S
Sao Tome	STO	6.7°E	0.0°N	7.5°W	2.5°N
S. Sulawesi	SUL	123.8°E	5.6°S	122.5°E	7.5°S
Tahiti	TAH	149.5°W	17.7°S	147.5°W	17.5°S
Tanzania	TAN	38.0°W	7.0°S	37.5°W	7.5°S
Tarawa	TAR	173.0°E	1.3°N	172.5°E	2.5°N

Table 1. (continued)

Location Name	Abbreviated Name	Longitude	Latitude	Grid Longitude	Grid Latitude
Thitu Isl	THI	114.3°E	11.0°N	112.5°E	12.5°N
Truk	TRU	151.9°E	7.4°N	152.5°E	7.5°N
Veracruz	VER	92.0°W	20.2°N	92.5°W	22.5°N
Yap	YAP	138.1°E	9.5°N	137.5°E	7.5°N
Yemen	YEM	43.1°E	13.9°N	42.5°E	12.5°E
Yongala Reef	YON	147.6°E	19.3°S	147.5°E	17.5°S

Data are from *Bryan* [1952] and International Center for Living Aquatic Resources Management (ReefBase: A global database on coral reefs and their resources, http://www.cgiar.org/iclarm/resprg/reefbase/, 1997).

imation is consistent with the goal of capturing large scale patterns of SST variability.

3.2. Temporal Resolution of Hypothetical Reconstructions

The literature describing the extraction of records of SST variability from corals reports weekly [*Gagan et al.*, 1994] to annual [*Dunbar et al.*, 1994] to biennial [*Druffel*, 1997] time series resolution. Here we assume that corals may be used to achieve monthly-resolution reconstructions of SST, and use monthly-resolution EOFs from *Kaplan et al.* [1998].

3.3. Number of SST EOFs Resolved by Coral Data

How many spatial patterns of SST variability may be resolved by our sparse network of hypothetical coral data? A priori we will assume that the $\leq$65 coral sites resolve no more SST anomaly structure than do the 80 EOFs [*Kaplan et al.*, 1998] describing 75% of SST anomaly variance. Equivalently, we assume that the EOF space sufficiently resolves the coral-based SST anomalies. The SST anomaly variance retained in these 80 patterns is summed and contoured in Figure 2; note that variance resolved in the analysis is greatest in the central and eastern equatorial Pacific, the North Pacific, and the North Atlantic.

3.4. Observational Error

R is the sum of observational error and space reduction terms (equation (6)). The observational error variance ϵ^2 is not the analytical error of the isotopic or chemical measurement; it is the error in obtaining SST estimates from the proxy measurement. We will assume ϵ is constant across coral sites and repeat the optimal site analysis for a range of ϵ from 0.1°-1.0°C to assess the sensitivity of the results to ϵ. We will allow for the possibility that resampling a site, rather than choosing a new site, minimizes $\mathbf{P}$, by assuming that noise in the coral data is uncorrelated between different time series reconstructions. Hence for n samples

$$\epsilon^2_{\text{resampled site}} = \epsilon^2_{\text{once sampled site}}/n. \tag{9}$$

3.5. Evaluation of the OI Error Covariance Matrix, P

With the parameters described above, $\mathbf{P}$ is an 80 $\times$ 80 matrix. To "minimize" $\mathbf{P}$, we need to choose a metric, i.e., a scalar function, of $\mathbf{P}$. For example, we might choose to minimize the mean squared error in an index, such as the average SST anomaly over some ocean region, such as the eastern tropical Pacific or the North Atlantic. This average can be written as

$$\text{index averaged error} = \mathbf{W^T E P E^T W} + \mathbf{W^T E' \Lambda' E'^T W} \tag{10}$$

where $\mathbf{W}$ is the diagonal matrix containing grid area weights with zero elsewhere [*Kaplan et al.*, 1997]. The error in the index average has two terms: the first is the error in the area average for the analyzed SST field, while the second is the error due to the EOF truncation; neither depends on the network of sites selected. If the average $\mathbf{W}$ are large in scale, then the small-scale errors (second term of (10)) will be small. Since our goal is the reconstruction of the large-scale features of global SST variability we will choose to minimize $\mathbf{P}$ as the mean squared error over all grid points as represented in the 80 EOFs of the reduced space, which is equivalent to minimization of the trace of $\mathbf{P}$:

$$\text{mean error} = \text{trace}(\mathbf{P}) = \sum_{i=1}^{80} P_{ii}. \tag{11}$$

where trace is the operator which sums the diagonal elements of a matrix. We also report networks which minimize the error in reconstruction of global, eastern tropical Pacific, and North Atlantic indices of SST variability, as well as the locations at which the 10 highest correlations with global mean SST (Bradley's criterion)

are found (Table 2). There we have listed the 10 grid boxes in the analysis of *Kaplan et al.* [1998] which have the highest individual correlations with the global mean SST, also from the *Kaplan et al.* [1998] analysis.

3.6. Approach to Minimization of P

Finding the best set of all possible combinations of M sites within a possible set of N locations, $N \gg M$, is computationally expensive. For instance, finding the best set of 10 sites by trying all possible combinations of 10 sites in 65 would require $O(10^{11})$ 80×80 element matrix inversions for **P**. Also, the question of the next best site is perhaps more relevant than the set of M best sites. Instead of evaluating **P** for all possible combinations of a small number of sites (full solution) we can consider the following question. Given a small number of sites, what is the additional site which most reduces the amplitude of our evaluation of **P** (sequential solution)? This approach to the evaluation of **P** acknowledges that in consideration of sites already sampled it may be of more interest to find the next best site than a set of best sites. Therefore we adopt this sequential approach, and compare the results for 1-10 and 65 sites with the results from the full solution for 3 and 6 sites.

4. Assumptions Made in This Analysis

The OI approach and parameter choices outlined in the preceding section incur several assumptions, which we briefly outline below before proceeding to a discussion of the results.

4.1. Coral Data: Assumptions

1. The coral proxy measurement is assumed to be solely a function of SST variability, including other influences insofar as they are highly correlated with local SST variability. Any bias in the linear relationship between SST anomaly and coral proxy anomaly is assumed to be removed prior to analysis. Nonlocal SST variability which may be reflected in coral proxy data through their dependence on other local climatological variables (e.g., rainfall) is not considered in this model, although it may be significant for SST field reconstruction.

2. Coral-based SST estimates represent SST variability in the $5^o\times5^o$ grid box in which they are located; in other words, we assume that the differences between pointwise SST recorded by the coral data and the $5^o\times5^o$ grid box mean is not correlated with SST at distant points and thus does not influence the large-scale SST analysis. We also assume that the 65 potential sites we consider in this analysis are inclusive of all possible sites and, conversely, that long-lived corals are recoverable from any of these sites. This last expectation may not be realistic, especially with distance away from the equator and outside of the ocean's warm pools [*Sorokin*, 1993; *ICLARM*, 1997].

3. Observational error in reconstruction of SST anomaly at a given site is uncorrelated with the observational error at other sites. This ought to be the case when the potential sites are well separated in space and when the observational errors are due to local or small-scale influences.

Table 2. Sites Selected for Different Minimization Criteria

ME		G		ETP		NA		BRA
ϵ=0.3°C	ϵ=0.7°C	ϵ=0.3°C	ϵ=0.7°C	ϵ=0.3°C	ϵ=0.7°C	ϵ=0.3°C	ϵ=0.7°C	
GAL	GAL	COC	TAR	GAL	GAL	CVI	CVI	CHI
KIR	KIR	NAU	COC	KIR	KIR	KAP	TAN	PEN
FEL	GYM	ROC	FEL	COC	GYM	SOM	KAP	COC
GYM	TAR	SPR	SPR	GYM	COC	BAR	CVI	LAK
CVI	FEL	FEL	NAU	TAH	GAL	ABR	FEL	FEL
REU	KAN	TAH	ROC	TAR	TAR	SEY	BAR	ROC
ASC	REU	PEN	GYM	FEL	KAN	BER	ABR	TAH
TAR	CVI	TRU	AND	STH	TAH	CVI	SOM	CLI
OKI	GAL	GYM	DGA	GAL	GAL	SOL	CVI	JAM
CHR	STH	REU	REU	KAN	COC	TAN	SOL	YEM

ME, trace(**P**); G, analysis error for estimation of SST averaged over the global oceans; ETP, analysis error for estimation of SST in the eastern tropical Pacific index region (150°-80°W, 25°N-25°S); NA, analysis error for estimation of SST in the North Atlantic index region (15°-60°W, 25°-80°N); and BRA, Bradley optimization criterion results (see text). Site names are abbreviated as in Table 1.

4. Coral data can capture monthly resolution SST variability. Age model uncertainty is included here only as an influence on the estimated observational SST error ϵ.

4.2. Model: Assumptions

1. The reduced space of 80 EOFs adequately represents the signal of interest, that is, the dominant patterns of large-scale SST variability.

2. The variance not resolved in the reduced EOF space has small decorrelation scales in both time and space. It is discarded in this analysis. This is consistent with our interest in capturing large-scale patterns of SST variability in the proxy data.

3. The covariance structures represented by the EOFs are stationary in time to the extent that the spatial covariance in preinstrumental SST variability may be adequately represented by some linear combination of the retained EOFs. Although this assumption is likely to be true for the largest-scale patterns which are likely to be resolved by proxy data over the past several hundred years, it may not hold over timescales through which fundamental climatic conditions have markedly varied.

4. The analysis domain (see Figure 1) provides near-global ocean coverage in the northern hemisphere; this is certainly not true for the southern hemisphere oceans poleward of 40°S, where there is insufficient data to construct the spatial covariances. Hereafter, "global" means are understood to be mean SST averaged over the analysis domain or roughly 40°S-60°N.

Some of the data assumptions are admittedly optimistic, especially with respect to temporal resolution and quality of the proxy data. In addition, model assumptions concerning error characteristics and stationarity of the spatial covariance captured in the EOFs should be explored further and will be the subject of further work. Many of these assumptions may also be tested via cross validation of historical SST data and contemporaneous coral-based proxy time series. When enough data have been collected to formulate more realistic assumptions, the present analysis can be modified to accomodate them.

We should also note that the goal of reconstruction of the preinstrumental large-scale SST variability is merely one of many interests of the coral paleoclimatological community (for an overview, see *Dunbar and Cole* [1993]). In this respect our results should not be considered as a blueprint for future coral research but rather should be placed within the larger context of coral-based paleoclimatological studies. Instead, we view the general approach described here as a tool to be used for the development of optimal sampling networks for geophysical or other field variables of interest.

5. Results and Discussion

First, we present two sets of results for sequential site selection of 3 and 10 sites, representative of the results obtained for ϵ = 0.1-1.0°C (Figures 3 and 4). The first set (Figure 3) shows the sites selected at a low observational error (ϵ = 0.3°C) level. The second set (Figure 4) shows the sites selected at higher observational error (ϵ = 0.7°C). Contours show the reduction in the error variance fields relative to the signal variance field captured by 80 EOFs (Figure 1):

$$(\text{error/signal} - 1) \times 100\%$$

where error = diag($\mathbf{EPE^T}$) is the error variance on the spatial grid (equation 8) and signal = diag($\mathbf{E\Lambda E^T}$) is the variance of the signal in the 80 EOFs projected onto the grid; diag is the operator which selects the diagonal elements of the resulting square matrices. These maps indicate the quality of the hypothetical coral reconstruction using the selected sites relative to the variance in the signal. For instance, a relative error reduction of 0% indicates that the reconstruction error at that location is equal in magnitude to the signal; a relative error reduction of 50% means that the analysis error has been reduced to half the size of the signal.

5.1. Optimal Site Selection

For a wide range of observational error the analysis always first picks the eastern equatorial Pacific (Galápagos grid box: 92.5°W, 2.5°S) and the central equatorial Pacific (Kiritimati grid box: 157.5°W, 2.5°N; Table 2). These sites are selected to capture the large SST anomaly variance associated with the El Niño-Southern Oscillation (ENSO) phenomenon. Additional site selection is sensitive to the observational error level; however, over the complete range of ϵ there were no differences between the "fully optimal" and "sequential" solutions for up to six sites (results not shown).

At low observational error variance (ϵ = 0.3°C; Figure 3a) the analysis seeks a third site distant from the previous two to explain other SST variance. The selected site is in the equatorial Indian Ocean (Felidhu grid box: 72.5°E, 2.5°N). Error reduction reaches 50% local to selected sites and is reduced by 10%-40% over much of the eastern tropical Pacific and the tropical Indian Ocean. At higher observational error (ϵ = 0.7°C; Figure 4a) the analysis reduces error by additional sampling in the eastern Pacific (now the third site selected is the Guaymas grid box: 112.5°W, 27.5°N). Error reduction is not as geographically extensive as it is for the low observational error case; it is mostly confined to the eastern tropical Pacific and is marginal in the tropical Indian Ocean.

For 10 sites and low observational error, additional error reduction is achieved by nonredundant sampling.

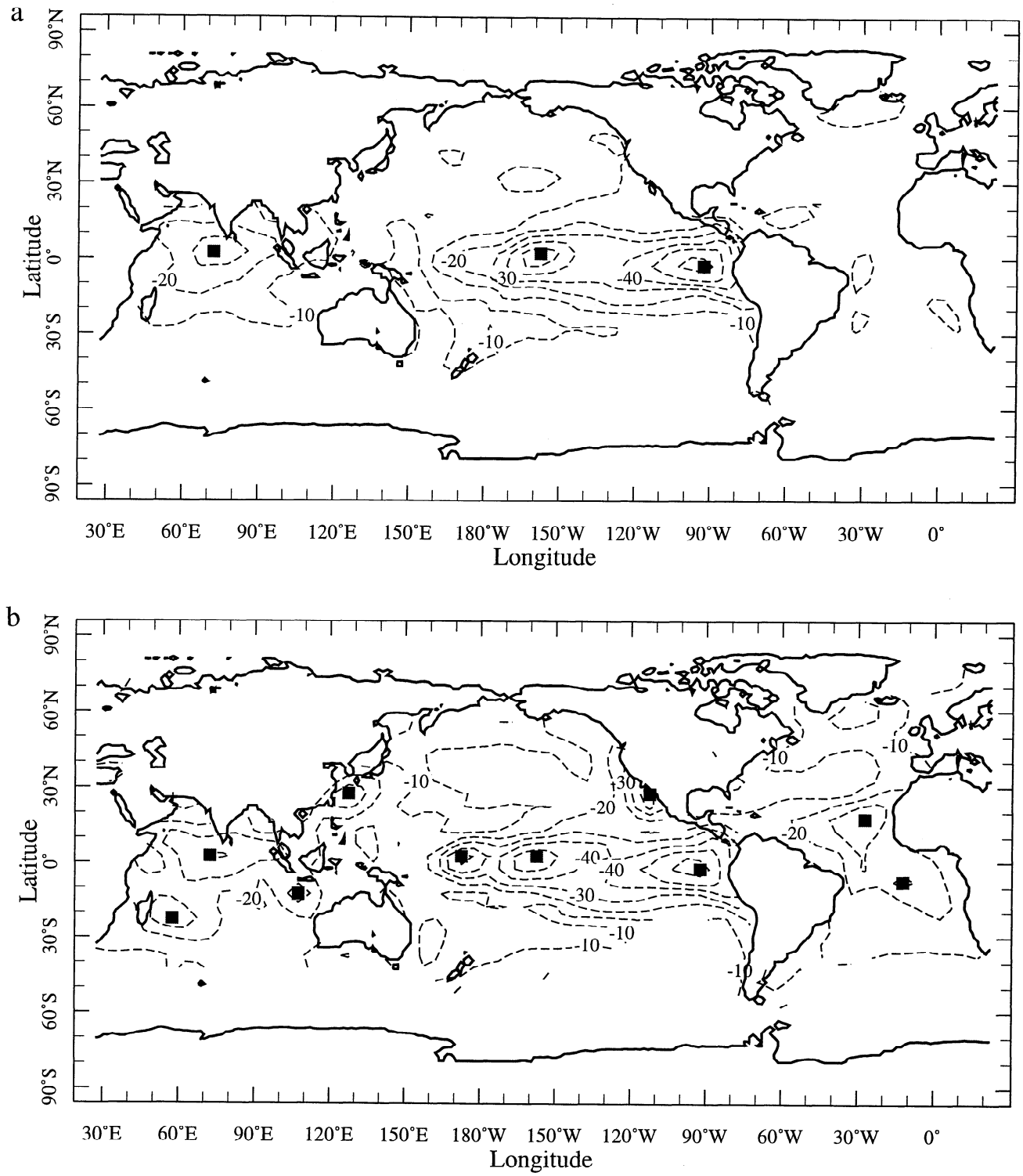

Figure 3. (a) Percent error reduction, relative to the RMS variance in 80 EOFs (Figure 2), for the best three sequentially chosen sites; observational error $c = 0.3°C$. Solid squares give selected site locations. (b) Same as Figure 3a, except for the first 10 sequentially chosen sites.

Sites are chosen in the equatorial Atlantic and subtropical Pacific (Figure 3b). However, at higher observational error the analysis relies on resampling of the most important sites to reduce best the analysis error. For example, the 10 sites chosen with $\epsilon = 0.7°C$ include twice sampling the Galápagos site and sampling of a site (Kanton grid box: 172.5°W, 2.5°S) near the second site chosen, Kiritimati (Figure 4b). However, despite

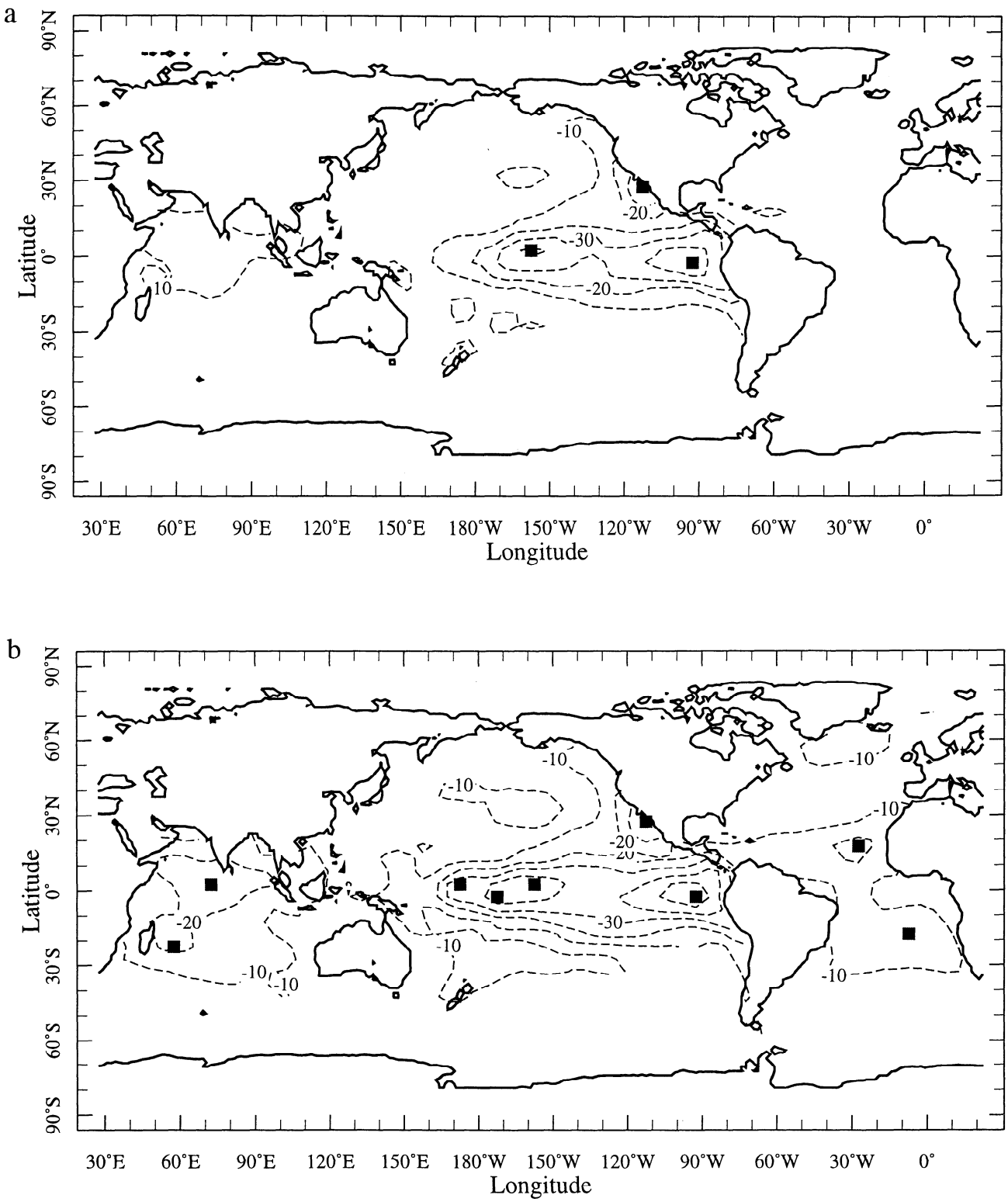

Figure 4. (a) Percent error reduction, relative to the RMS variance in 80 EOFs (Figure 2), for the best three sequentially chosen sites; $\epsilon = 0.7°C$. Solid squares give selected site locations. (b) Same as Figure 4a, except for the first 10 sequentially chosen sites.

the sensitivity of the optimal network design to the observational error level, only 15 of the possible 65 sites were chosen over the entire range of $\epsilon^2(0.01^o\text{-}1.0^oC^2)$ studied.

5.2. Error Reduction in Index Averages

We have also computed the error reduction achieved in index regions of the world's oceans (see (10)). Recall that the sites chosen are optimized only for the global RMS error (trace(**P**)). Figure 5a shows results for the global RMS error (as in Figures 3 and 4), and Figures 5b, 5c, and 5d show the error in estimation of the three indices, eastern tropical Pacific (ETP) SST (25°N-25°S, 150°-80°W), North Atlantic (NA) SST (25°-80°N, 15°-60°W), and global mean (G) SST, respectively, as a function of the number of sites sequentially sampled. Results for the two representative levels of observational error used in Figures 3 and 4 are shown: $\epsilon = 0.3^oC$ (solid line) and $\epsilon = 0.7^oC$ (dashed line). Mean error reduction (Figure 5a) smoothly decreases with additional site sampling. Deeper error reduction in the low ϵ case than for the higher ϵ case (Figure 4a) is expected as the analysis is better able to resolve the covariance patterns. However, most of the error reduction in the ETP region is achieved with just three sites (Galápagos, Kiritimati, and Guaymas); additional sites reduce the ETP index error only marginally. In the NA index, error reduction is almost nil, until the fifth site (Cape Verde Islands: grid box 27.5°W, 17.5°N) is sampled with low ϵ; at high ϵ, error reduction is very small, even if all 65 sites are sampled once. This is because no sites are located near or in the index region and, even at low ϵ, only a small amount of covariance with selected sites exists. Error in construction of the global mean SST index decreases smoothly with site, reaching ≈50% of the variance in this index (Figure 5d), and is surprisingly large considering the limited number and geographical extent of coral sites. Overall, however, much of the error reduction in the analysis is driven by and confined to error reduction in the tropical oceans, especially the high-variance regions of the eastern equatorial Pacific (Figure 2; compare Figure 4a to Figure 4b).

5.3. Error Reduction for Other Minimization Criteria

The results described to this point are for optimal coral networks which minimize the mean error in the 80 EOFs resolved by the analysis. If, as mentioned earlier, we choose a different metric for minimization of **P**, we obtain different site networks. Some examples of networks resulting from minimization of the global mean, eastern tropical Pacific, and North Atlantic SST anomaly are given in Table 2. These networks represent cases in which the desired reconstruction is of the largest spatial scale (G), has high SST anomaly variance (ETP), or is remotely located relative to the sampling sites (NA), respectively. We find that the global minimization criterion produces a network composed of central and eastern tropical Pacific sites, with additional sites selected in the northern Indian Ocean and the tropical Atlantic. This network is similar to that achieved when minimization is to produce the smallest error in the ETP region, although additional sites chosen are mainly previously sampled central and eastern tropical Pacific sites. Minimization with respect to North Atlantic SST anomaly reconstruction suggests a coral network composed of sites in the tropical Atlantic but also includes sites in the western Indian Ocean and the western equatorial Pacific. The approach of *Bradley* [1996] implemented for the global mean SST criterion results in similar site selection as in our approach to the minimization of the global mean SST (Table 2); however, the Bradley sites are not optimal since the sites chosen in our analysis result in a lower error in reconstruction of the global SST (results not shown). Overall, these results suggest that while the exact location of sites chosen will depend on the desired reconstruction, an optimal set of sites will detect both the signal of interest and the large-scale patterns of SST anomaly that covary with it.

5.4. Error Reduction as a Function of the Parameters in P

Figure 6 shows results for mean error reduction (equation (11)) as a function of the observational error and the number of sites selected for a wide range of ϵ. For comparison we also show the average mean error for the period 1861-1900 from the optimal interpolation (OI) SST analysis of *Kaplan et al.* [1998]. Figure 6 illustrates the general results of our optimal network analysis.

5.4.1. Size of the network. Not surprisingly, the mean analysis error decreases with increasing number of sites. If no sites are selected, the mean error is given by the dotted line in Figure 6: the OI solution is zero, and **P** is equal to $\mathbf{\Lambda}$, the magnitude of the variance of the signal. When all 65 sites are sampled once, error reduction reaches 16% -30% of the variance, depending on ϵ (Figure 6, dashed line). The 65-site level of error is an estimated limit on the quality of any coral-based global SST reconstruction, although at moderate and high observational error levels (e.g., above 0.6°C; Table 2), redundant sampling will lower the analysis error somewhat further.

5.4.2. Amplitude of ϵ^2. When ϵ^2 is small relative to $\mathbf{\Lambda}$ and $\mathbf{\Lambda}'$, **P** becomes a function of **H** and the EOF space reduction. Essentially, the location of the measurement sites determines the quality of the SST field reconstruction, and the differences between the information provided by each site is most distinct. In this case the solution will converge on reconstruction

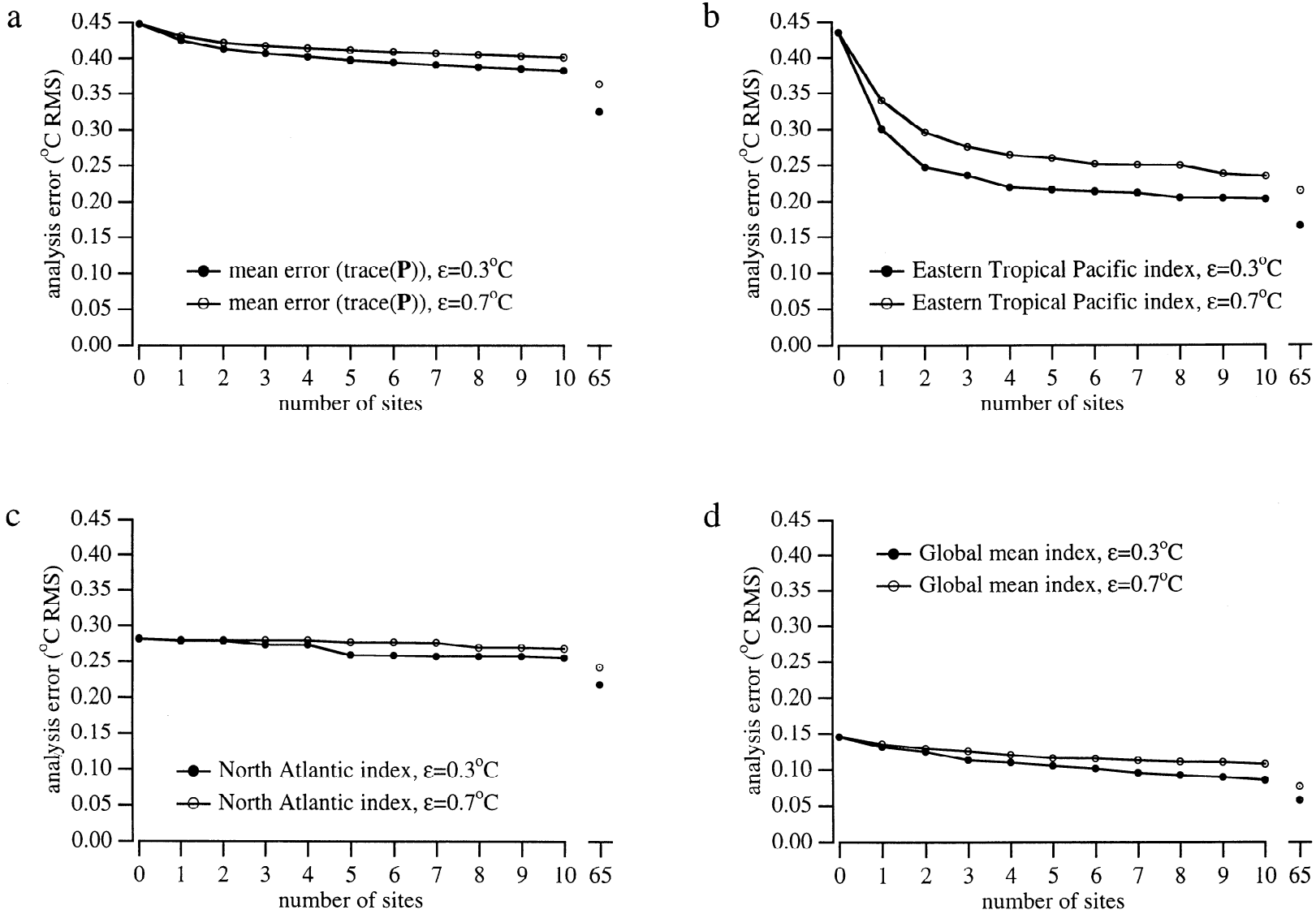

Figure 5. Error reduction in the estimation of index area SST averages as a function of the number of sites sampled: (a) mean error reduction (see text), (b) eastern tropical Pacific index (25°N-25°S, 150°-80°W) error reduction, (c) North Atlantic index (25°-80°N, 15°-60°W) error reduction, and (d) global mean SST error reduction. Solid circles give results for $\epsilon = 0.3°C$; open circles give results for $\epsilon = 0.7°C$.

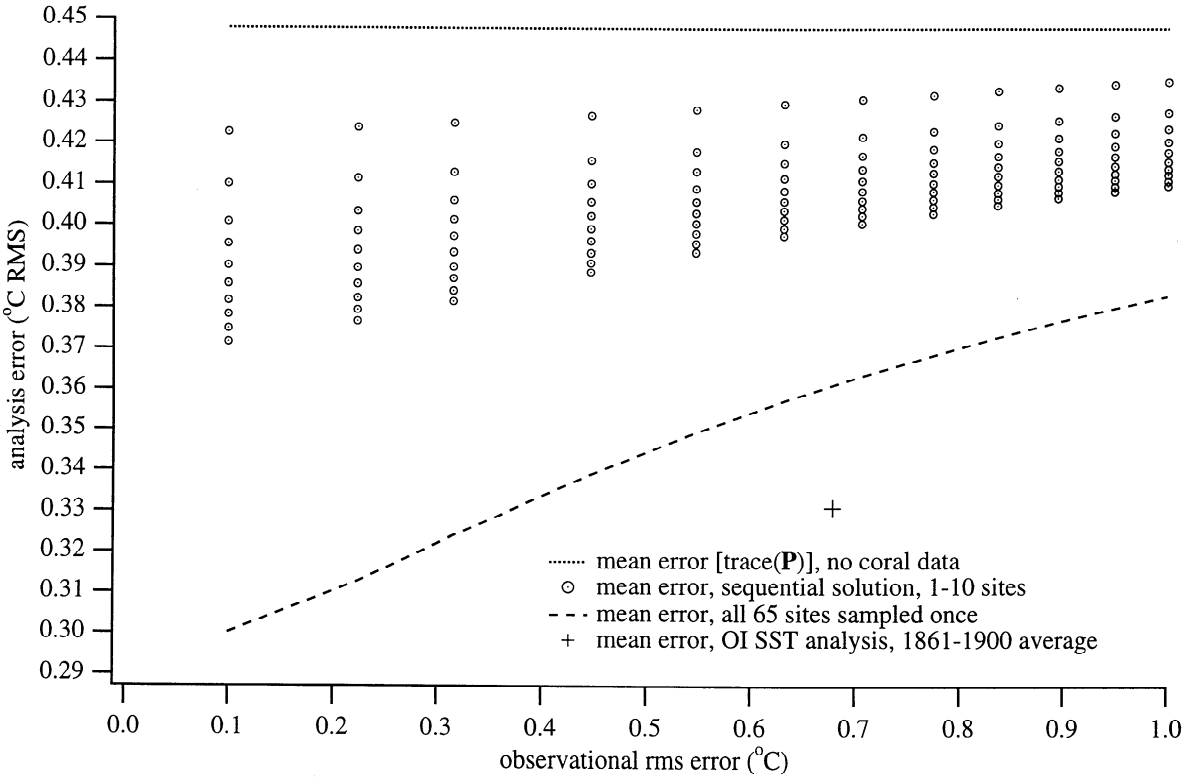

Figure 6. Mean error reduction in the reduced EOF space as a function of the number of sites sequentially sampled and the observational error ϵ. The dotted line is mean error in the analysis with no sites selected ($\sqrt{\text{trace}(\mathbf{P})} = 0.45°\text{C}$). Error reduction for single sampling of all 65 potential sites is shown as a dashed line. The average mean error for the optimal interpolation SST analysis by *Kaplan et al.* [1998] for 1861-1900 is 0.3°C and is shown for comparison (cross). Average optimal interpolation (OI) SST analysis errors for 1901-1940 and 1951-1990 are 0.2° and 0.1°C, respectively.

of the information contained in the 80 EOFs as additional sites are selected. Figure 3 shows that small ϵ allows error reduction in subtropical regions quite remote from the coral sites, because of the resolution of $\mathbf{E}$. More likely, we will find that ϵ^2 is large relative to the discarded variance $\mathbf{\Lambda}'$. When ϵ^2 is large relative to $\mathbf{\Lambda}'$, but still small relative to $\mathbf{\Lambda}$, additional site selection will still capture more variance, although the quality of the reconstruction will be poorer than in the small-ϵ^2 case. In addition, the difference between the analysis error achieved by the optimal site and other sites will be smaller than before; thus the exact location of the site becomes less critical. Comparison of annually averaged (April-March) SST anomaly data from *Kaplan et al.* [1998] and coral δ^{18}O data from the past century from Tarawa Atoll and Kiritimati Island indicates that ϵ is in this range ($\epsilon \approx 0.4°$-$0.5°$C). When ϵ is large relative to both $\mathbf{\Lambda}'$ and $\mathbf{\Lambda}$, error reduction depends on obtaining smaller ϵ by resampling sites; monthly averages of the coral data mentioned produce ϵ estimates in this range ($\epsilon \approx 0.6°$-$0.7°$C). In the results shown in Figure 4, error reduction is confined to the central and eastern equatorial Pacific, equatorial Indian Ocean, and Atlantic warm pool core regions, adjacent to the sampling sites chosen. Thus, while reconstructions using coral data with low ϵ will recover pantropical and limited extratropical information, higher ϵ will confine useful reconstruction results to the equatorial and tropical oceans.

5.5. Marginal Return on Additional Sites

Figure 6 also shows that there is a diminishing return with increasing number of sites sampled with little dependence on ϵ. The error reduction achieved by the 2 sites, Kiritimati and Galápagos, is half the error reduction of 10 sites; the error reduction by 6-7 sites is about half the error reduction achieved by single sampling of all 65 sites in the analysis. These results suggest that a limited coral data set of low-ϵ time series from critical locations may extract almost as much information about past SST variability as will a much more expansive, and expensive, network of sites. On the other hand, we also note that a network composed of all 65 sites sampled at very low ϵ (e.g. $\epsilon \leq 0.3°$C) may reduce the analysis RMS error to the level of that achieved by the historical SST analysis during the poorest period of observational SST coverage, 1861-1900; the global mean analysis error for this period is 0.3°C (Figure 6). In summary, the analysis suggests that annually averaged

coral data from only a handful of sites with sufficiently small ϵ may be used to reconstruct large-scale patterns of SST variability for the preinstrumental period with reasonably low analysis error.

6. Conclusion

We have derived sparse networks of sites for reconstruction of the global SST field. This is accomplished by minimizing the error in an optimal interpolation analysis of global SST anomaly as a function of observational error and observation site given a reduced space statistical model of the spatial covariance of sea surface temperature anomaly. We estimate observational error variance ϵ^2 for SST derived from proxy measurements on corals but analyze results for a wide range of ϵ. For the complete range of observational error variance ϵ examined, central and eastern equatorial Pacific coral sites best minimize the mean error in a hypothetical global SST field reconstruction from coral data. If the observational error is sufficiently low, additional sites are chosen in the equatorial Indian and Atlantic Oceans and selected subtropical locations. If ϵ is large, the analysis suggests that the best approach to minimizing the error is to reduce the observational error by resampling the most important sites. The marginal return on additional sites diminishes rapidly and is not sensitive to ϵ: 2 sites reduce the analysis error by half as much as 10 sites, while the first 6-7 sites achieve half the error reduction of all 65 sites in the analysis domain. For index-averaged regions such as the eastern tropical Pacific the first two sites selected produce most of the error reduction; more remote index regions, such as the North Atlantic, require additional sites but reduce the error far less. Networks of sites derived using other analysis error minimization criteria pick different sites but underline the importance of the equatorial oceans, especially the Pacific and the Indian Oceans. These results suggest that a limited set of sites with low ϵ ($\approx$ 0.3-0.6°C) will provide the best approach to SST field reconstruction from coral data.

Acknowledgments. R. Fairbanks first attracted our attention to this problem. We are grateful to J. McManus of the International Center for Living and Aquatic Resource Management (ICLARM) for making ReefBase 2.0 available over the Internet. The manuscript was improved by the comments of J. Lough, J. Chiang, and M. Delaney and by the reviews of T. Quinn and two anonymous referees. Funding was provided by NOAA grants UCSIO-10075411D/NA47GPO-188. LDEO contribution 5813.

References

Barth, N., and C. Wunsch, Oceanographic experiment design by simulated annealing, *J. Phys. Oceanogr.*, *20*, 1249–1263, 1990.

Bennett, A. F., Inverse methods in assessing ship-of-opportunity networks and estimating circulation and winds from tropical expendable bathythermograph data, *J. Geophys. Res.*, *95*, 16,111–16,148, 1990.

Bennett, A. F., *Inverse Methods in Physical Oceanography*. Cambridge Univ. Press, New York, 1992.

Bottomley, M., C. K. Folland, J. Hsiung, R. E. Newell, and D. E. Parker, *Global Ocean Surface Temperature Atlas*. Her Majesty's Str. Off., Norwich, England, U.K., 1990.

Bradley, R. S., Are there optimum sites for global pal-eotemperature reconstruction?, in *Climatic Variations and Forcing Mechanisms of the Last 2000 Years, NATO ASI Ser. I, Global Environmental Change*, edited by P. D. Jones, R. Bradley, and J. Jouzel, vol. 41, pp. 603–624, Springer-Verlag, New York, 1996.

Bretherton, F. P., and J. C. McWilliams, Estimations from irregular arrays, *Rev. Geophys.*, *18*, 789–812, 1980.

Bretherton, F. P., R. E. Davis, and C. B. Fandry, A technique for objective analysis and design of oceanographic experiments applied to MODE-73, *Deep Sea Res.*, *23*, 559–582, 1976.

Bryan, E. H., Check list of Atolls, *Atoll Res. Bull.*, *19*, 1–38, 1952.

Cane, M. A., A. Kaplan, R. N. Miller, B. Tang, E. C. Hackert, and A. J. Busalacchi, Mapping tropical Pacific sea level: Data assimilation via a reduced state space Kalman filter, *J. Geophys. Res.*, *101*, 22,599–22,617, 1996.

Cane, M. A., A. C. Clement, A. Kaplan, Y. Kushnir, R. Murtugudde, D. Pozdnyakov, R. Seager, and S. E. Zebiak, 20th century sea surface temperature trends, *Science*, *275*, 957–960, 1997.

Charles, C. D., D. E. Hunter, and R. G. Fairbanks, Interaction between the ENSO and the Asian monsoon in a coral record of tropical climate, *Science*, *277*, 925–928, 1997.

Darwin, C., *The Structure and Distribution of Coral Reefs*, Univ. of Calif. Press, Berkeley, 1962.

Druffel, E. R. M., Pulses of rapid ventilation in the North Atlantic surface ocean during the past century, *Science*, *275*, 1454–1457, 1997.

Dunbar, R. B., and J. E. Cole, *Coral Records of Ocean-Atmosphere Variability: Report From the Workshop on Coral Paleoclimate Reconstruction*, NOAA, La Parguera, Puerto Rico, 1993.

Dunbar, R. B., G. M. Wellington, M. W. Colgan, and P. W. Glynn, Eastern Pacific sea surface temperature since 1600 A.D.: The $\delta^{18}O$ record of climate variability in Galápagos corals, *Paleoceanography*, *9*, 291–315, 1994.

Evans, M. N., R. G. Fairbanks, and J. L. Rubenstone, A proxy index of climate teleconnections from the central equatorial Pacific, *Nature*, in press, 1998.

Gagan, M. K., A. R. Chivas, and P. J. Isdale, High-resolution isotopic records from corals using ocean temperature and mass-spawning chronometers, *Earth Planet. Sci. Lett.*, *121*, 549–558, 1994.

Ghil, M., and P. Malanotte-Rizzoli, Data assimilation in meteorology and oceanography, *Adv. Geophys.*, *33*, 141–266, 1991.

Ghil, M., S. Cohn, J. Tavantzis, K. Bube, and E. Isaacson, Applications of estimation theory to numerical weather prediction, in *Dynamic Meteorology: Data Assimilation Methods*, vol. 36, *Applied Mathematical Sciences*, edited by L. Bengtsson, M. Ghil, and E. Kallen, pp. 139–224, Springer-Verlag, New York, 1981.

Hackert, E. C., R. N. Miller, and A. J. Busalacchi, An optimized design for a moored instrument array in the tropical Atlantic Ocean, *J. Geophys. Res.*, *103*, 7,491–7,509, 1998.

Hayes, S. P., J. Mangum, J. Picaut, A. Sumi, and K. Takeuchi, TOGA-TAO: A moored array for real-time measurements in the tropical Pacific Ocean, *Bull. Am. Meteorol. Soc.*, *72*, 339–347, 1991.

Kaplan, A., Y. Kushnir, M. A. Cane, and M. B. Blumenthal, Reduced space optimal analysis for historical datasets: 136 years of Atlantic sea surface temperatures, *J. Geophys. Res.*, *102*, 27,835–27,860, 1997.

Kaplan, A., M. A. Cane, Y. Kushnir, A. C. Clement, M. B. Blumenthal, and B. Rajagopalan, Analyses of global sea surface temperature 1856-1991, *J. Geophys. Res.*, in press, 1998.

McPhaden, M. J., G. Reverdin, J. Merle, Y. Du Penhoat, and A. Kartavtseff, Objective analysis of simulated equatorial Atlantic Ocean data on seasonal time scales, *Deep Sea Res., Part A*, *31*, 551–569, 1984.

Miller, R. N., Tropical data assimilation experiments with simulated data: The impact of the Tropical Ocean and Global Atmosphere thermal array for the ocean, *J. Geophys. Res.*, *100*, 13,389–13,425, 1990.

Quinn, T. M., T. M. Crowley, F. W. Taylor, C. Henin, P. Joannot, and Y. Join, A multicentury stable isotope record from a New Caledonia coral: Interannual and decadal SST variability in the southwest Pacific since 1657, *Paleoceanography*, in press, 1998.

Sorokin, Y. I., *Coral Reef Ecology*. Springer-Verlag, New York, 1993.

M. A. Cane, M. N. Evans, and A. Kaplan, Lamont-Doherty Earth Observatory, RT 9W, Palisades, NY 10964-8000. (email: mcane@ldeo.columbia.edu; mevans@ldeo.columbia.edu; alexeyk@ldeo.columbia.edu)

(Received February 2, 1998;
revised June 17, 1998;
accepted June 23, 1998.)